Journal of
Polymer Materials

Tech Science Press

http://doi.org/10.32604/jpm.2026.086454

ARTICLE

Preparation and Application of Polystyrene Microspheres as Plugging Agents in Water-Based Drilling Fluids

Boxuan Wu[1], Mei-Chun Li[1,2,3,*], Yang Ding[1] and Chaozheng Liu[4]

[1]School of Petroleum Engineering, China University of Petroleum (East China), Qingdao, China
[2]State Key Laboratory of Deep Oil and Gas, China University of Petroleum (East China), Qingdao, China
[3]Shandong Key Laboratory of Oil and Gas Field Chemistry, China University of Petroleum (East China), Qingdao, China
[4]Co-Innovation Center of Efficient Processing and Utilization of Forest Resources, College of Materials Science and Engineering, Nanjing Forestry University, Nanjing, China
*Corresponding Author: Mei-Chun Li. Email: mli@upc.edu.cn

Received: 30 May 2026; Accepted: 22 July 2026; Published: 24 September 2026

ABSTRACT: Severe fluid loss in fractured formations remains a critical challenge in drilling operations, often leading to wellbore instability and increased non-productive time. Conventional plugging materials typically suffer from limited size adaptability and insufficient sealing efficiency under high-temperature conditions. To address these challenges, this study developed a plugging agent based on polystyrene microspheres (PSMs) via dispersion polymerization, using polyvinylpyrrolidone (PVP) as a dispersant. By tuning the molar ratio of PVP to styrene monomer, PSMs with controllable particle sizes (0.12–1.34 μm) were successfully synthesized. The results indicate that PSMs prepared at a PVP/SM molar ratio of 0.01, with an average particle size of ~0.28 μm, exhibited optimal plugging performance. Through a synergistic bridging-filling mechanism, these microspheres reduced the invasion depth into sand beds by over 40%. The addition of 2 wt% PSMs decreased the API fluid loss of the drilling fluid from 25.0 mL to 17.0 mL after aging at 120°C for 16 h, while simultaneously forming a denser filter cake. Furthermore, the incorporation of PSMs significantly enhanced the cuttings suspension capacity of the drilling fluid. This study provides a promising strategy for designing high-performance plugging agents for formations dominated by micro-fractures.

KEYWORDS: Drilling fluid; fractured formation; plugging agent; polystyrene microsphere; fluid loss

1 Introduction

As global oil and gas exploration advances into deep fractured reservoirs, the invasion of drilling fluid filtrate along micro- and nanoscale pore throats and natural microfractures has emerged as a primary trigger for wellbore instability, formation damage, and severe lost circulation [1,2]. Particularly in deep (>4500 m) and ultra-deep environments, the coupled effects of high *in situ* stress, elevated temperatures (120–200°C), and strong heterogeneity render conventional drilling fluid systems incapable of constructing a long-term stable, low-permeability plugging barrier at the wellbore–formation interface [3–6]. Achieving efficient, size-matched plugging of micro- and nanoscale pores and fractures within water-based drilling fluids (WBDFs), while simultaneously ensuring thermal resistance, dispersion stability, and cost-effectiveness for field-scale application, constitutes a critical technical bottleneck restricting safe and efficient deep-well drilling operations [7].

Current lost circulation material (LCM) systems are mainly classified into two categories: rigid plugging agents and flexible plugging agents. Rigid plugging agents include conventional rigid particles (e.g.,

calcium carbonate and graphite) and inorganic nanomaterials (e.g., nano-SiO_2, nano-TiO_2, and nanoclay). Conventional rigid particles rely on particle stacking to form a physical barrier, but suffer from difficulties in controlling particle size distribution and are prone to fragmentation under high-temperature and high-pressure conditions [8]. Inorganic nanomaterials, by virtue of their nanoscale effects, can reduce fluid invasion depth by filling micropores in the filter cake and nanopores in shale reservoirs [9,10]. However, their hydrophilicity readily induces flocculation and agglomeration, resulting in poor dispersion stability in the drilling fluid environment [11,12]. Furthermore, purely rigid nanomaterials lack deformation adaptability, which limits their effectiveness in sealing multiscale fractures with a wide aperture distribution [13]. On the other hand, flexible plugging agents (e.g., emulsified asphalt and polymer gels) rely on the deformation of molecular chains to seal fractures [13]. For example, Lei et al. [14] designed a latex plugging agent with self-crosslinking functionality, whose plugging performance was further enhanced after heat treatment. Although these methods have achieved significant improvements in plugging strength, they are generally accompanied by complex preparation processes, high raw material and synthesis costs, and increased uncertainty arising from competitive adsorption or flocculation with other additives in water-based drilling fluids due to the introduction of surface functional groups [12].

In recent years, shape memory polymers (SMPs) have emerged as promising high-performance lost circulation materials (LCMs) for reservoir sealing. Unlike conventional rigid or flexible LCMs, SMPs can be programmed into compact temporary configurations, facilitating their injection into fractures. Upon exposure to downhole temperatures, they recover their original expanded geometry, thereby effectively sealing fractures of various widths. This thermomechanical programming enables SMPs to undergo a substantial reduction in size before deployment, with the programmed dimensions being up to an order of magnitude smaller than their original shape. Consequently, SMPs can be readily transported through flow lines and subsequently expand to bridge wide fractures under reservoir conditions [15]. Compared with conventional LCMs, SMPs can significantly reduce the risk of downhole tool blockage while improving plugging performance [16,17]. Despite these advantages, several limitations still hinder their widespread application, including: (i) the requirement for precise matching of the activation temperature to the downhole environment; (ii) relatively high material and synthesis costs; (iii) pumping challenges arising from their viscoelastic properties; and (iv) a primary focus on sealing large fractures rather than reducing matrix permeability over a broader scale.

Against this technological backdrop, polystyrene (PS) particles exhibit considerable application potential owing to their unique physicochemical properties [18]. As a classical polymer material, PS offers good chemical stability, tunable particle size, and distinct advantages in terms of low cost and scalability for mass production [19]. As one of the most widely produced general-purpose plastics worldwide, PS benefits from the broad availability and low cost of its monomer, styrene (approximately 12,000 RMB per ton). Furthermore, PS particles can be efficiently synthesized via facile radical polymerization under mild conditions (60–80°C, atmospheric pressure), enabling kilogram-scale production without complex post-processing [20]. This production cost is significantly lower than that of alternative materials, such as nanoclays or nano-silica, which often require energy-intensive high-temperature calcination [21–23]. More importantly, the chemical inertness of PS ensures its stability in water-based drilling fluids over a pH range of 4–10 [24–26]. This property minimizes the risk of adverse side reactions with other drilling fluid additives and prevents performance degradation caused by chemical bond cleavage, which is common in certain chemically modified materials [27]. Furthermore, the particle size can be readily tailored by controlling the reaction parameters, resulting in enhanced size adaptability and improved sealing efficiency.

This study focuses on the controllable synthesis and performance optimization of monodisperse polystyrene microspheres (PSMs). PSMs with tunable particle sizes were synthesized by adjusting the molar ratio of PVP to styrene monomer during polymerization. Their performance as plugging agents in water-based drilling fluids was systematically evaluated, with emphasis on sand-bed invasion depth, filtration performance. Furthermore, the effect of PSMs on the rheological performance of drilling fluids was evaluated. This work establishes a low-cost, scalable strategy for designing size-tunable polymer microspheres that enable efficient and thermally stable micro-nano plugging in water-based drilling fluids, thereby advancing reliable wellbore sealing in formations dominated by micro-fractures.

2 Experimental

2.1 Materials

The chemical reagents include styrene (≥99%, Shanghai Macklin Biochemical Co., Ltd.), polyvinylpyrrolidone (PVP, $M_W \geq 40{,}000$, Shanghai Aladdin Biochemical Technology Co., Ltd.), sodium carbonate (≥99%, Shanghai Aladdin Biochemical Technology Co., Ltd.) and potassium persulfate (KPS, ≥99%, Shanghai Macklin Biochemical Co., Ltd.). Bentonite was obtained from Tengfei Co., Ltd. (Huai'an, China). Deionized water was prepared in-house. All chemicals were used as received without further purification.

2.2 Synthesis of PSMs

The detailed synthesis procedure is schematically illustrated in Fig. 1a. First, 0.06 g (0.11 g or 0.57 g) of PVP was dissolved in 100 mL of deionized water, followed by the addition of 11.44 g of styrene monomer. Notably, the dispersion exhibited no appreciable phase separation during the 15 min period after stirring was stopped. Furthermore, optical microscopy analysis (Fig. 1b) revealed that the styrene (St) monomer droplets remained uniformly dispersed throughout the aqueous phase. These observations indicate that even at the lowest PVP/St molar ratio (0.005), the PVP concentration was sufficient to provide transient colloidal stabilization of the dispersion prior to polymerization. The mixture was then transferred to a three-necked flask and deaerated with nitrogen for 30 min. Subsequently, the solution was heated to 70°C under continuous stirring at 500 rpm. A total of 10 g of KPS solution (0.15 g KPS dissolved in 9.85 g water) was then added dropwise to initiate polymerization. The reaction was maintained at this temperature for 4 h. The synthesis follows a dispersion polymerization mechanism, in which the water-soluble initiator potassium persulfate (KPS) generates free radicals in the aqueous phase, leading to homogeneous nucleation. As the growing polystyrene chains become insoluble, they precipitate to form primary polymer particles, while polyvinylpyrrolidone (PVP) adsorbs onto their surfaces and acts as a steric stabilizer, preventing particle aggregation and ensuring colloidal stability throughout the polymerization process. After completion, the resulting PSM suspension was cooled naturally to room temperature. The samples were collected by centrifugation and washed three times with ethanol to remove residual monomers. The purified product was then redispersed in deionized water via ultrasonication and subsequently lyophilized to obtain the final PSMs. During the synthesis, the molar ratios of PVP to SM were adjusted to 0.005, 0.01, and 0.05. The corresponding samples were denoted as 0.005PSM, 0.01PSM, and 0.05PSM, respectively. After lyophilization, the dried PSMs were weighed to determine the polymerization yield. The polymerization yield was calculated as the ratio of the mass of the recovered PSMs to the initial mass of styrene monomer charged into the reaction.

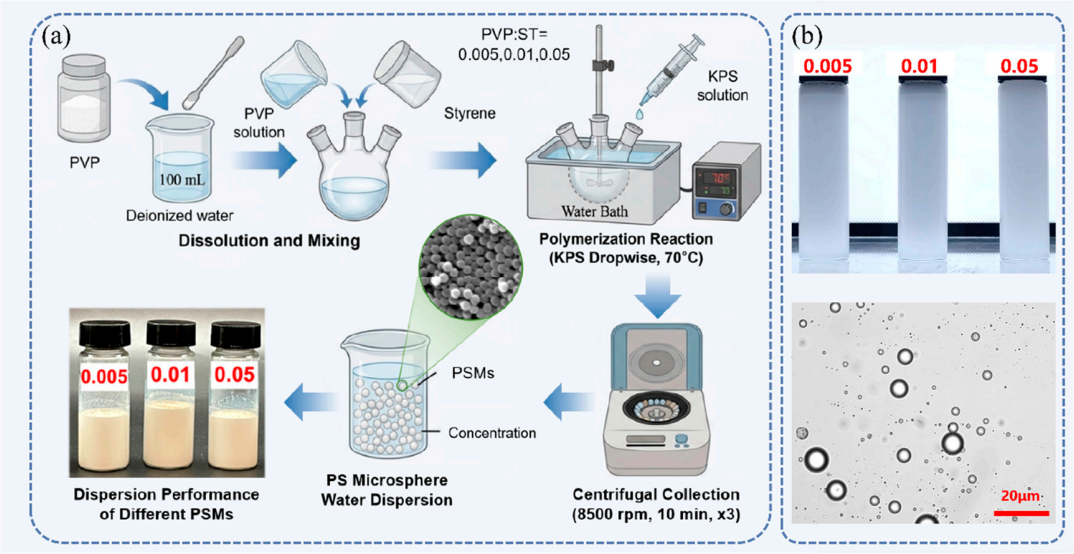

Figure 1: (**a**) Schematic illustration of the PS microspheres synthesis process; (**b**) Macroscopic and microscopic images of the pre-polymerization PVP/St dispersion after 15 min of static incubation.

2.3 Preparation of Based Mud (BM) and PSMs-Modified BM

Bentonite was dispersed in deionized water at a mass fraction of 4 wt% and stirred at 3000 rpm for 1 h. The resulting slurry was then aged at room temperature for 24 h to obtain bentonite-based mud (BM). Subsequently, PSMs were added to the BM and mixed at 2000 rpm for 1 h to prepare water-based drilling fluids containing PSMs. The mass ratios of PSMs to BM were set at 0.5:100, 1:100, and 2:100, and the corresponding samples were denoted as BM-0.5PSMs, BM-1PSMs, and BM-2PSMs, respectively.

2.4 Characterization of PSMs

The morphology of the PSMs was characterized using a scanning electron microscope (SEM; EVO-15/LS, Zeiss, Germany). The samples were ultrasonically dispersed in deionized water at a concentration of 0.005 g/mL. A droplet of the suspension was deposited onto conductive adhesive tape, naturally dried at room temperature, and subsequently mounted on an aluminum stub. To enhance conductivity, a thin conductive layer (Au, approximately 10 nm thick) was deposited onto the sample surface via sputter coating. SEM imaging was performed under high-vacuum conditions with an accelerating voltage of 20 kV and a working distance (WD) of approximately 8 mm.

The particle size distribution of the PSMs was determined using a laser diffraction analyzer (Mastersizer 3000, Malvern, UK). The samples were dispersed in deionized water to obtain suspensions with a concentration of 0.05 g/mL for measurement. The stirred dispersion was introduced into the sample chamber until the turbidity (optical obscuration) reached 5%–10%. Measurements were conducted under stirring with an impeller rotating at approximately 2500 rpm. The refractive index of the microsphere material was set to n = 1.59 (with the imaginary component representing absorption fixed at 0.01), while the refractive index of the dispersant was defined as 1.33 (water). Each sample was measured in triplicate.

Fourier transform infrared (FTIR) spectroscopy (IRTracer-100, Shimadzu, Japan) was employed to identify functional groups and chemical bonds. Prior to analysis, the PSMs were thoroughly mixed with potassium bromide (KBr), finely ground, and pressed into transparent pellets at 1.5 MPa for 2 min. The spectra were recorded over a wavenumber range of 400–4000 cm^{-1}.

The zeta potential, reflecting the surface charge characteristics of the particles, was measured using a Zetasizer Nano ZS90 (Malvern, UK). Samples were dispersed in deionized water at a concentration of 0.05 g/mL, sonicated for 1 min, and then loaded into a folded capillary cell (DTS1070). Measurements were performed at 25°C with an equilibration time of 120 s. Each sample was measured in triplicate.

2.5 Plugging Performance of PSM-Modified BM

The plugging performance of the PSM-modified drilling fluids was evaluated using a visual medium-pressure sand-bed plugging apparatus (Model FA.BX, Qingdao Tongchun Petroleum Instrument Co., Ltd.). Drilling fluid samples containing different PSM loadings were introduced into the apparatus packed with 140–160 mesh quartz sand. A pressure of 0.7 MPa was applied, and the invasion depth of the drilling fluid was recorded after a static period of 30 min.

2.6 Rheological and Filtration Performance of PSM-Modified BM

The rheological properties of BM with varying PSM contents were measured using a six-speed rotational viscometer (ZNN-D6, China). The samples were tested at rotational speeds of 600 and 300 rpm, and the corresponding dial readings were recorded. The apparent viscosity (AV), plastic viscosity (PV), and yield point (YP) were calculated according to the following equations [28]:

$$AV = \frac{1}{2}\theta_{600} \tag{1}$$

$$PV = \theta_{600} - \theta_{300} \tag{2}$$

$$YP = 0.511(\theta_{300} - PV) \tag{3}$$

where θ_{600} and θ_{300} represent the readings taken at rotational speeds of 600 and 300 rpm, respectively.

A roller oven (CW300 PLC, China) was used to perform the thermal aging tests. The drilling fluid samples were transferred into aging cells and aged at 120°C under continuous rolling (200 rpm) for 16 h. After aging, the samples were allowed to cool to room temperature before further characterization.

The filtration performance was evaluated using a standard API filter press (Model SD, Qingdao Tongchun Petroleum Instrument Co., Ltd.). Filtration tests were conducted at room temperature under a nitrogen differential pressure of 100 psi for 30 min, and the filtrate volume was recorded at the end of each test. The resulting filter cakes were carefully removed, dried at 60°C to constant weight, and weighed to determine their solid content. In addition, the surface morphology of the filter cakes was characterized by scanning electron microscopy (SEM; ZEISS EVO-15/LS) to evaluate the filter-cake densification induced by the PSMs.

3 Results and Discussion

3.1 Synthesis and Characterization of PSMs

PSMs were synthesized via dispersion polymerization, and their morphology and size were systematically tuned by varying the molar ratio of PVP to styrene monomer. The resulting samples were characterized by SEM, as shown in Fig. 2a–c. All samples exhibit well-defined spherical morphology with smooth surfaces and good structural integrity, indicating the successful formation of PSMs. No obvious aggregation or deformation is observed, suggesting that PVP effectively stabilized the particles during polymerization. Notably, the measured polymerization yields for 0.005PSM, 0.01PSM, and 0.05PSM after 4 h of polymerization

were 74.3%, 87.7%, and 91.4%, respectively. These values, calculated as the mass ratio of recovered PSMs to the initial styrene monomer feed after purification (washing, centrifugation, and lyophilization), are slightly lower than the true monomer conversion due to material losses during the purification steps. The results indicate that a reaction time of 4 h at 70°C is sufficient to achieve high monomer conversions (>85%) for 0.01PSM and 0.05PSM. The relatively lower conversion of 0.005PSM is likely attributable to reduced colloidal stability at the lowest PVP concentration, which promotes the formation of small amounts of polymer deposits on the reactor walls and stirrer during polymerization. Furthermore, because the PSMs were subsequently purified by repeated ethanol washing followed by freeze-drying, the residual styrene monomer content in the final dried product is expected to be negligible.

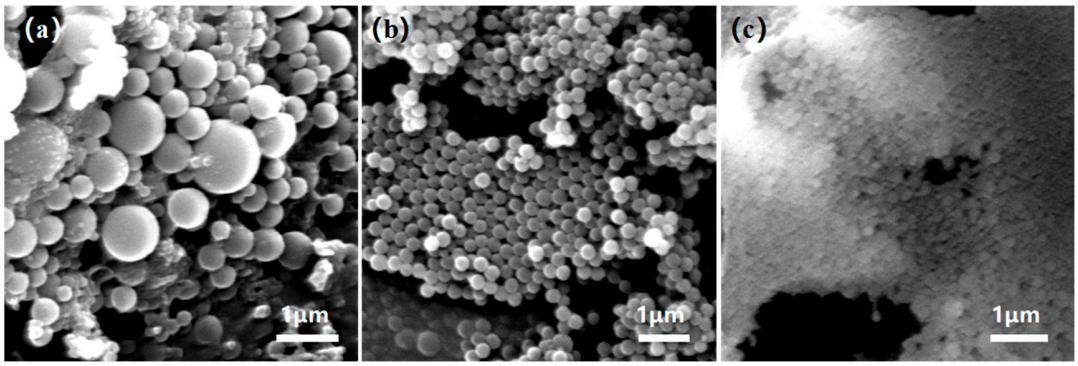

Figure 2: SEM of PSMs prepared with different molar ratios of PVP to styrene: (**a**–**c**) SEM image of 0.005PSM (**a**), 0.01PSM (**b**), and 0.05PSM (**c**).

The particle size distributions of the PSMs were measured using a laser diffraction particle size analyzer. The median particle diameters (D50, Fig. 3a), 0.005PSM, 0.01PSM, and 0.05PSM were 0.631 μm, 0.215 μm, and 0.132 μm, respectively. The complete particle size distribution (PSD) curves are provided in Figs. S1–S3 (Supplementary Material). As summarized in Fig. 3a, the particle size decreases progressively with increasing PVP/SM molar ratio, demonstrating that the particle size of PSMs can be precisely regulated by adjusting the dispersant content. This tunability is critical for achieving size-matched plugging in multiscale pore-fracture systems.

The observed size evolution can be attributed to the role of PVP as a steric stabilizer during polymerization. PVP molecules adsorb onto the surface of nascent polymer nuclei, forming a protective layer that suppresses particle coalescence and secondary aggregation [29]. As the PVP concentration increases, more stabilizing chains are available to cover newly formed nuclei, leading to a higher number of effective nucleation sites in the early stage of the reaction [30]. Under a fixed monomer dosage, the available styrene is thus distributed among a larger number of growing particles, resulting in smaller final particle sizes. In addition, the enhanced steric hindrance provided by PVP further limits particle growth through collision and fusion, contributing to the formation of uniform and narrowly distributed microspheres. Overall, these results confirm that the PVP/SM ratio serves as a key parameter governing nucleation and growth processes, enabling controllable synthesis of PSMs with tailored sizes for targeted plugging applications.

The surface charge of the PSMs was evaluated in terms of their zeta potential. As shown in Fig. 3b, all PSM samples exhibit negative zeta potential values, which indicates the incorporation of negatively charged groups during the synthesis process. Specifically, sulfate radicals (SO_4^{2-}) generated from the thermal decomposition of the initiator, potassium persulfate (KPS), can attach to the microsphere surface, forming negatively charged sulfate or sulfonate groups [31]. Furthermore, although PVP is a nonionic polymer, it

can induce an apparent negative surface charge due to the strong polarity of its pyrrolidone groups. The carbonyl groups preferentially attract OH^- ions and modify the interfacial double-layer structure, thereby increasing the effective negative zeta potential [32]. Consequently, even in the absence of ionic surfactants, PS microspheres typically carry a net negative surface charge.

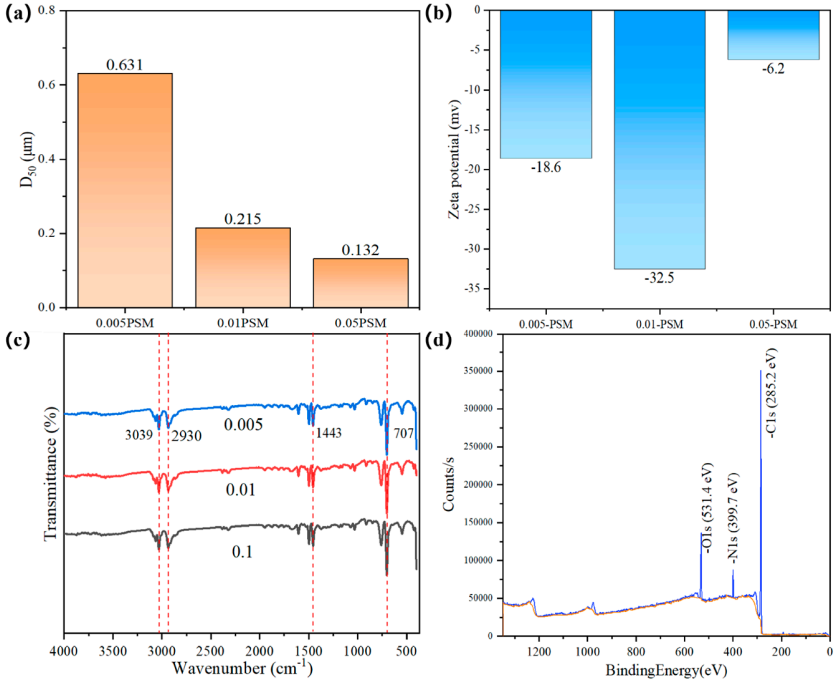

Figure 3: Characterizations of PSMs prepared with different molar ratios of PVP to styrene: (**a**) D50 particle size; (**b**) Zeta potential; (**c**) FTIR spectra; (**d**) XPS spectra of various PSMs.

Notably, the zeta potential of the PSMs exhibits a distinct non-monotonic dependence on the PVP/styrene molar ratio. As the ratio increases from 0.005 to 0.01, the zeta potential decreases significantly from −18.6 mV to −32.5 mV, indicating an increase in surface charge density and enhanced electrostatic repulsion between particles. This behavior can be associated with the presence of PVP on the particle surface. The highly polar pyrrolidone groups in PVP can modify the interfacial double-layer structure, while the hydrophilic chains extending into the aqueous phase facilitate the preferential adsorption of OH^- ions, thereby increasing the effective negative surface charge density [33]. Under these conditions, the system achieves optimal dispersion stability. However, when the PVP/styrene ratio is further increased to 0.05, the zeta potential rises markedly to −6.2 mV. At this higher concentration, excess PVP not only fully covers the particle surfaces but also remains in the continuous phase. The presence of abundant free polymer chains increases the solution viscosity and compresses the electrical double layer, partially shielding the surface charges and leading to a significant reduction in the absolute zeta potential value [33]. Consequently, the dominant stabilization mechanism shifts from electrostatic repulsion to steric hindrance, which explains the relatively poorer dispersibility observed for the 0.05PSM sample (Fig. 2c).

Fig. 3c presents the FTIR spectra of the three PSMs. All spectra display characteristic absorption bands of polystyrene, confirming the successful synthesis of PSMs and indicating that the core chemical structure remains essentially unchanged with varying PVP/styrene ratios. The high degree of overlap among the spectra further suggests that PVP does not participate in the polymerization reaction but primarily acts as a physical stabilizer during particle formation. Specifically, the absorption bands at approximately 3039 cm^{-1}

and 2930 cm^{-1} are attributed to the stretching vibrations of aromatic C-H bonds on the benzene ring and aliphatic C-H bonds in methylene groups, respectively. The peaks near 1600 and 1443 cm^{-1} correspond to the skeletal stretching vibrations of the benzene ring and in-plane C-H bending vibrations. The sharp and intense peak at ~707 cm^{-1} is assigned to the out-of-plane bending vibrations of adjacent hydrogen atoms on a monosubstituted benzene ring, serving as a definitive fingerprint of the polystyrene structure. In addition, weak or broad features that appear in the region of 1650–1700 cm^{-1} can be associated with the C=O stretching vibration of the pyrrolidone group in PVP, indicating the presence of PVP on the particle surface. However, owing to the low PVP loading and the bulk-sensitive nature of FTIR spectroscopy, this signal alone is insufficient to conclusively confirm the presence of PVP on the microsphere surface. Therefore, X-ray photoelectron spectroscopy (XPS) was employed to provide surface-sensitive evidence. The XPS survey spectrum (Fig. 3d) exhibits three principal peaks corresponding to C 1s (285.2 eV), O 1s (531.4 eV), and a distinct N 1s peak at 399.7 eV. Quantitative analysis revealed surface atomic concentrations of 82.71 at% C, 10.43 at% O, 6.60 at% N, and 0.26 at% S. The characteristic N 1s peak at 399.7 eV, originating from the pyrrolidone nitrogen in PVP, provides direct evidence for the presence of PVP on the PSM surface, confirming its successful adsorption.

Overall, these results demonstrate that variations in PVP content mainly influence particle size, surface characteristics, and dispersion stability, rather than altering the intrinsic chemical structure of the polystyrene matrix. This finding is consistent with the role of PVP as a steric stabilizer that regulates nucleation and growth processes without modifying the fundamental polymer framework.

3.2 Optimization of PSMs as Plugging Agents

A visual medium-pressure sand-bed plugging apparatus was employed to evaluate the plugging performance of the three PSMs and to identify the optimal formulation. Quartz sand with a particle size of 140–160 mesh was used to construct the sand bed, providing a representative porous medium for simulating fluid invasion into formation pores.

The experimental procedure was as follows: the three PSMs were individually added to bentonite-based mud (BM) at a concentration of 0.5 wt%, yielding the modified drilling fluids denoted as BM-0.005, BM-0.01, and BM-0.05, respectively. These fluids, along with the base BM, were subjected to thermal aging at 120°C for 16 h to simulate downhole conditions. Subsequently, a transparent acrylic tube was uniformly packed with the quartz sand and compacted to ensure consistent porosity and permeability. After packing, 200 mL of each drilling fluid was introduced into the tube, and the invasion behavior was evaluated under a constant pressure of 0.69 MPa for 30 min. The invasion depth of the drilling fluid into the sand bed was recorded as a key indicator of plugging performance.

Fig. 4a illustrates the effect of PSM incorporation on the plugging performance of the drilling fluids. From left to right, the samples correspond to BM, BM-0.005, BM-0.01, and BM-0.05. The experimental results demonstrate that BM-0.01PSM (Fig. 4a(iii)) exhibits the most effective plugging performance (Fig. 4c), as evidenced by a significantly reduced invasion depth compared with BM-0.005PSM (Fig. 4a(ii)) and BM-0.05PSM (Fig. 4a(iv)).

This superior performance can be attributed to the optimal matching between particle size and the pore throat distribution of the sand bed, as well as the formation of a dense and continuous packing structure. According to classical particle packing and bridging theories, effective plugging occurs when particle sizes are comparable to the pore openings, enabling both mechanical bridging at pore throats and subsequent filling of interstitial voids. In the case of BM-0.005PSM, the relatively large particles are unable to penetrate into the pore network and instead form isolated bridges across larger channels. However, such mono-sized

bridging structures contain abundant unfilled macropores, preventing the formation of a low-permeability barrier. As a result, drilling fluid can still flow through the interparticle voids within the bridging framework, leading to limited plugging efficiency (Fig. 4c(i)).

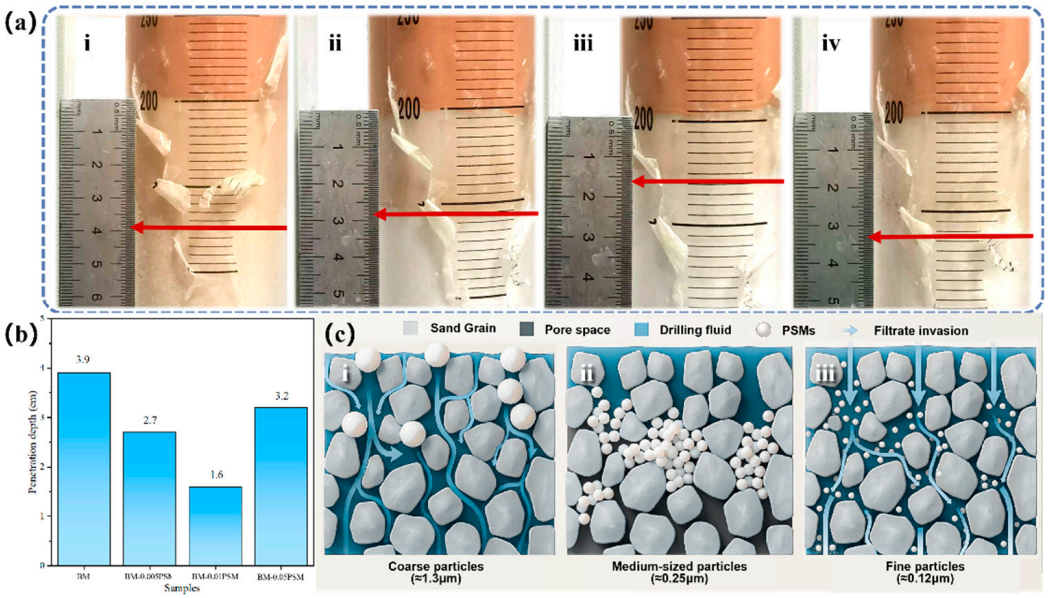

Figure 4: Plugging performance of PSMs: (**a**,**b**) invasion depth of drilling fluids into the sand bed after the addition of different types of PSMs (0.5 wt%); (**c**) schematic illustration of the mechanism governing the influence of particle size on plugging performance.

In contrast, although BM-0.05PSM contains smaller particles that can readily access finer pores, its plugging performance is compromised in the highly permeable sand bed. The small particles tend to migrate rapidly with the fluid phase, and their weak resistance to hydrodynamic forces promotes fingering and preferential channeling. Consequently, continuous leakage pathways are formed through the particle assembly (Fig. 4c(iii)) [34,35].

By comparison, the medium-sized microspheres in BM-0.01PSM fall within the optimal size range for simultaneously achieving bridging and filling. Under the applied pressure differential, these particles effectively accumulate at pore throats to form a stable bridging framework, while smaller interstitial voids are progressively filled by subsequent particles (Fig. 4c(ii)) [36]. Meanwhile, interparticle van der Waals interactions and mechanical interlocking further promote the formation of a compact and continuous filter cake. This hierarchical structure significantly increases flow tortuosity and resistance, thereby suppressing fluid invasion into the porous medium [37].

Overall, the superior performance of BM-0.01PSM arises from a synergistic mechanism involving size matching, efficient bridging, and dense packing, enabling the construction of a low-permeability barrier with minimal invasion depth. These findings highlight the critical importance of particle size optimization in designing effective plugging agents for multiscale porous formations. Therefore, 0.01PSM was identified as the optimal plugging agent and selected for subsequent experimental investigations.

3.3 Effect of PSM Loading on Filtration Performance

Upon incorporation into the drilling fluid, PSMs co-deposit with other solid phases on the wellbore wall to form a filter cake, thereby contributing to the sealing of formation pores and fractures. As illustrated in

Fig. 5a-d, the surface morphology of the filter cake undergoes a pronounced evolution with increasing PSM concentration from 0 to 2 wt%. The filter cake formed by the base mud without PSMs exhibits a rough and loosely packed structure with numerous well-developed pore (Fig. 5a), indicating poor sealing capability. With the addition of a small amount of PSMs (0.5 wt% and 1 wt%), progressive particle accumulation and stacking are observed on the filter cake surface (Fig. 5b,c), leading to partial pore filling and a reduction in surface roughness. At a higher PSM concentration of 2 wt%, a continuous and compact particle layer is formed (Fig. 5d), effectively covering and sealing the surface pores. This morphological transition suggests that PSMs undergo interfacial enrichment and preferential deposition under the applied pressure gradient, promoting the formation of a denser and more uniform filter cake.

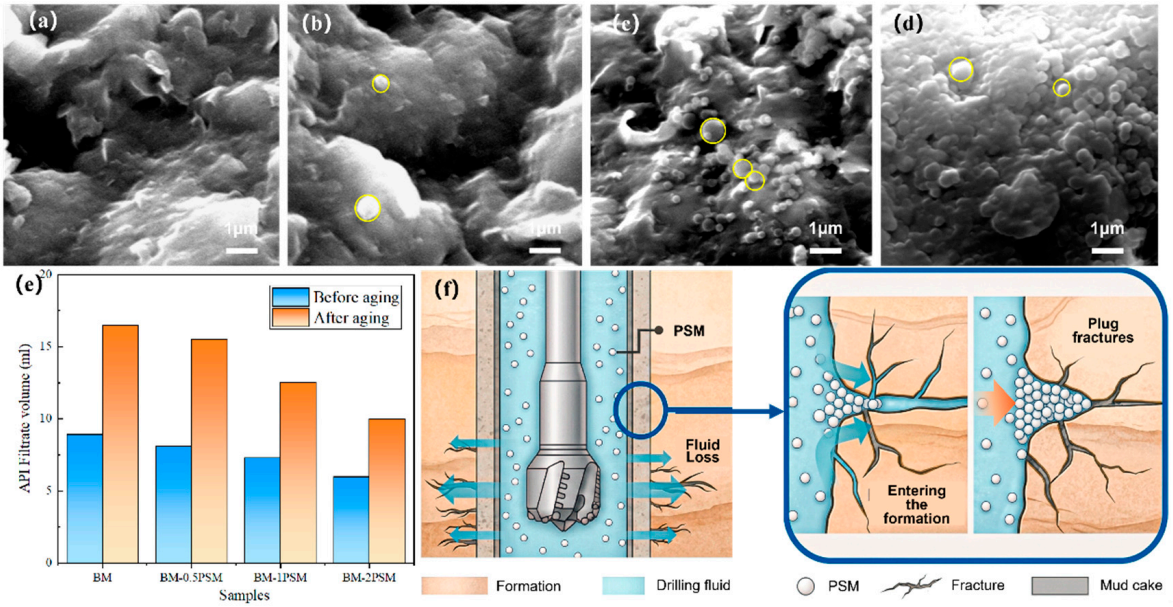

Figure 5: Filtration performance of drilling fluids containing different contents of PSMs: (**a**–**d**) morphology of filter cakes with different PSM loadings of (**a**) 0 wt%, (**b**) 0.5 wt%, (**c**) 1 wt%, and (**d**) 2 wt%; (**e**) effect of PSM concentration on API fluid loss; (**f**) schematic illustration of the plugging mechanism of PSMs in drilling fluids.

The API filtration results presented in Fig. 5e further confirm that the incorporation of PSMs significantly improves the fluid-loss control performance of the drilling fluid. Both before and after high-temperature aging, the filtrate volume decreases monotonically with increasing PSM concentration. For example, prior to aging, the filtrate volume is reduced from 9.8 mL for the base mud to 6.6 mL for the BM-2PSM formulation. More importantly, after aging at 120°C for 16 h, the filtrate volume of BM-2PSM (~17.0 mL) remains substantially lower than that of the aged base mud (~25.0 mL), demonstrating the excellent thermal stability of the PSM-modified system. This improvement can be attributed to the ability of submicron PSMs to penetrate and block the micro- and nanopores within the filter cake matrix. By filling interstitial voids between larger solid particles, PSMs reduce the effective permeability and promote the formation of a thinner, denser, and less permeable filter cake.

Furthermore, to further validate performance under extreme conditions, additional HTHP filtration tests were conducted (3.5 MPa, 160°C). A marked inverse correlation was observed between PSM loading (0–2 wt%) and fluid loss (decreasing from 89.5 mL to 43 mL), robustly substantiating that the PSMs retain plugging integrity at 3.5 MPa and 160°C (Fig. S4).

As illustrated in Fig. 5f, the PSMs are transported into the microfractures by the fluid flow, where they progressively bridge the pore throats and subsequently accumulate to form a dense plugging layer. This bridging-filling synergy effectively disrupts continuous flow pathways and significantly increases the tortuosity of the fluid migration channels. As a result, the resistance to fluid flow is markedly enhanced, thereby suppressing filtrate invasion into the formation. Overall, PSMs simultaneously reinforce the compact structure of the filter cake through interfacial deposition and establish an efficient physical barrier within pore-fracture networks. This dual mechanism underlies their effectiveness in reducing fluid loss and maintaining long-term stability in high-temperature drilling environments.

3.4 Effect of PSM Loading on Rheological Properties

Rheological properties are one of the most pivotal parameters for evaluating drilling fluid performance, as they fundamentally govern wellbore cleaning and cuttings transport efficiency during drilling operations [38,39]. To systematically investigate the influence of PSMs on these critical properties, the apparent viscosity (AV), plastic viscosity (PV), and yield point (YP) were measured for both freshly prepared and high-temperature-aged drilling fluid systems.

Fig. 6a–c shows that increasing PSM concentration induces a synergistic evolution in the rheological behavior of the drilling fluid, characterized by an increase in AV, a decrease in PV, and a pronounced increase in YP. Specifically, as the PSM concentration increases from 0 to 2 wt%, the AV of the unaged fluid rises from 6.5 to 9.0 mPa·s, the PV decreases from 5.75 to 3.0 mPa·s, and the YP increases significantly from 0.75 to 6.0 Pa. A similar trend is observed after high-temperature aging, indicating that the effect of PSMs is robust under thermal conditions.

This rheological evolution can be attributed to the dual functional role of PSMs in the fluid system. On one hand, the smooth surfaces of the microspheres reduce interparticle friction and sliding resistance within the shear field, leading to a decrease in PV and thus lower flow resistance during circulation. On the other hand, PSMs act as structural reinforcement units that promote the formation of a particle-supported network through steric interactions and physical contacts, particularly after thermal aging. This network enhances the yield stress and structural strength of the fluid, as reflected by the substantial increase in YP, which is essential for improving the suspension and transport of drilled cuttings [40].

According to the rheological relationships, although PV decreases moderately, the increase in YP is much more significant and therefore dominates the overall increase in AV. This indicates that the incorporation of PSMs effectively shifts the fluid behavior toward a more structured, yield-stress-dominated system. Such a rheological profile is advantageous for drilling operations, as it balances low resistance to flow under high shear conditions with strong suspension capacity under static or low-shear conditions.

Moreover, the persistence of these trends after high-temperature aging suggests that PSMs contribute to mitigating the thermal degradation of conventional polymer–clay networks. By forming a thermally stable, physically interconnected particulate skeleton, PSMs help maintain the integrity and functionality of the drilling fluid under harsh downhole conditions. Overall, these results demonstrate that PSMs not only enhance filtration control but also optimize rheological performance, providing a synergistic improvement in drilling fluid functionality.

3.5 Potential Limitations of PSMs in Complex Downhole Environments

All experiments in this study were conducted under idealized aqueous conditions. However, in actual deep reservoirs, drilling fluids may come into contact with acidic gases (e.g., CO_2 and H_2S) and crude oil, which may adversely affect the chemical stability and dispersion behavior of PSMs.

To evaluate the effects of CO_2 on the dispersibility of PSMs, the following experiments were performed. PSM particles were dispersed in deionized water at a concentration of 3 wt% and ultrasonicated for 15 min to ensure homogeneous dispersion, yielding an aqueous PSM suspension with an initial pH of approximately 7 (Fig. 7a). CO_2 was continuously bubbled through the suspension using a corrosion testing apparatus until the pH decreased to approximately 5.5 and 3.5, after which microscopic images were recorded (Fig. 7b,c). The observations showed that significant agglomeration of the PSM particles occurred when the pH reached 3.5. This behavior is likely attributable to the substantial reduction in the zeta potential of the PVP-coated PS particles under acidic conditions (pH < 5), which weakens electrostatic repulsion and promotes particle aggregation. In addition, the steric stabilization provided by the PVP layer may also be diminished under strongly acidic conditions. In deep reservoirs containing acidic gases (CO_2 and H_2S) under high-pressure (>10 MPa) and high-temperature (80–150°C) conditions, the pH of formation water or wellbore condensate may decrease to 3–5 under moderate acid gas concentrations and even to as low as 2.7 in highly sour gas reservoirs [41]. Therefore, the presence of CO_2 and H_2S may reduce the local pH near the wellbore sufficiently to induce premature agglomeration of PSMs, thereby compromising their plugging performance.

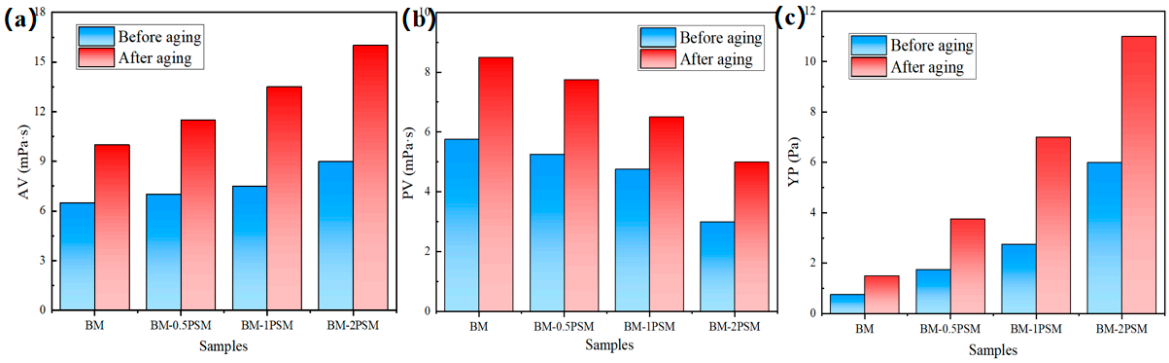

Figure 6: Rheological properties of drilling fluids containing different contents of PSMs: (**a**) AV, (**b**) PV and (**c**) YP.

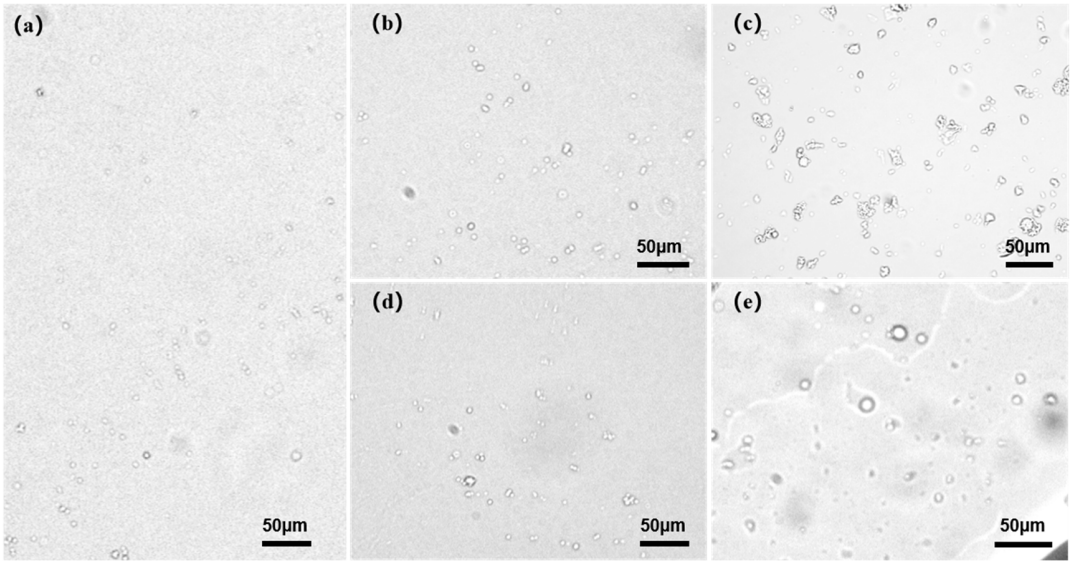

Figure 7: Influence of CO_2 and white mineral oil on the dispersion stability of PSMs. Digital photographs showing the dispersibility of PSMs: (**a**) in aqueous medium at pH ≈ 7; (**b**) at pH ≈ 5.5; (**c**) at pH ≈ 3.5; (**d**) after the introduction of 3 wt% white mineral oil; and (**e**) after the introduction of 6 wt% white mineral oil.

Furthermore, to evaluate the effect of oil contamination on the dispersibility of PSMs, white mineral oil was added to the aqueous PSM suspension at concentrations of 3 wt% and 6 wt%, respectively. After stirring for 30 min followed by static settling for 15 min, microscopic images were acquired to examine the dispersion state (Fig. 7d,e). The results indicate that the dispersibility of the PSMs remained essentially unchanged with increasing white mineral oil concentration, suggesting that oil contamination at the investigated concentrations has a negligible effect on their dispersion stability.

Although this study demonstrates the potential of PSMs as plugging agents for water-based drilling fluids, their application in hydrocarbon-bearing and acidic gas-rich reservoirs still requires comprehensive validation under representative downhole conditions. Ongoing research in our group is focused on addressing these challenges through systematic environmental exposure tests and targeted material modifications to enhance their long-term stability and field applicability.

4 Conclusion

In this study, monodisperse polystyrene microspheres (PSMs) were successfully synthesized via a facile dispersion polymerization strategy by tuning the molar ratio of polyvinylpyrrolidone (PVP) to styrene monomer. The results demonstrated that 0.01PSM (~0.28 μm) achieved an optimal balance among particle size, surface charge, and dispersion stability, exhibiting a zeta potential of −32.5 mV and forming a homogeneous and stable colloidal system. When incorporated into water-based drilling fluids, PSMs acted as efficient physical plugging agents. The medium-sized 0.01PSM exhibited favorable matching with the pore-throat dimensions of the sand bed, enabling a synergistic bridging-filling mechanism that reduces the invasion depth by more than 40% compared with poorly matched particles. Increasing the PSM concentration further enhanced filtration control performance: at a dosage of 2 wt%, the API fluid loss decreased from 25.0 mL to 17.0 mL after aging at 120°C for 16 h, accompanied by the formation of a thinner and more compact filter cake. The incorporation of PSMs also induced a favorable rheological profile characterized by reduced plastic viscosity and significantly enhanced yield point, enabling lower flow resistance during circulation while markedly improving cuttings suspension capacity. Although the proposed system exhibits several notable advantages, it is not without limitations. These include its sensitivity to reservoir pore-size heterogeneity and the uncertainty of its performance under high-salinity and ultra-high-temperature conditions. Future studies should therefore focus on evaluating the plugging performance of PSMs under high-temperature/high-pressure conditions representative of downhole environments, including higher differential pressures and complex brines containing acidic gases. In addition, targeted material modifications to enhance acid resistance are essential for ensuring the long-term stability and plugging performance of PSMs in sour gas reservoirs.

Acknowledgement: The authors gratefully acknowledge the financial support provided by the Oil & Gas Major Project (2025ZD1401302), the National Natural Science Foundation of China (52474021), and the Jiangsu Specially-Appointed Professor Program.

Funding Statement: This work was supported by the Oil & Gas Major Project (2025ZD1401302), National Natural Science Foundation of China (52474021), and the Jiangsu Specially-Appointed Professor Program.

Author Contributions: Boxuan Wu: Methodology, Data Curation, Formal Analysis, Writing—Original Draft. Mei-Chun Li: Supervision, Investigation, Formal Analysis, Resources, Project Administration, Writing—Review & Editing. Yang Ding: Methodology, Validation, Software. Chaozheng Liu: Conceptualization, Supervision, Writing—Review & Editing. All authors reviewed and approved the final version of the manuscript.

Availability of Data and Materials: Supplementary information and supporting data are available from the corresponding author upon reasonable request.

Ethics Approval: Not applicable.

Conflicts of Interest: The authors declare no conflicts of interest.

Supplementary Materials: The supplementary material is available online at https://www.techscience.com/doi/10.32604/jpm.2026.086454/s1.

References

1. Xie G, Lv X, Bai Y, Huang D, Zhang L. Investigation on the plugging mechanism of nanocomposite polyacrylate copolymers in water-based drilling fluids: Experiments and applications. Geoenergy Sci Eng. 2024;242:213223. [CrossRef].
2. Tian Y, Liu X, Liu Y, Dong H, Zhang G, Su B, et al. Research and evaluation of a nanometer plugging agent for shale gas horizontal wells. ACS Omega. 2024;9(42):42698–708. [CrossRef].
3. Pang S, Xuan Y, Zhu L, An Y. Zwitterionic polymer grafted nano-SiO2 as fluid loss agent for high temperature water-based drilling fluids. J Mol Liq. 2025;417:126542. [CrossRef].
4. Guo Y, Yang X, Wang R, Zhao M, Wang J, Xie J, et al. Environmentally friendly and temperature resistant water-based drilling fluids with highly inhibitory synthetic nanocellulose polymers for deep sea drilling. Geoenergy Sci Eng. 2024;241:213196. [CrossRef].
5. Liu F, Zhang Z, Liao B, Sun J, Khan MA, Li MC. Recent advances in phase change microcapsules for oilfield applications. Adv Geo-Energy Res. 2025;16(3):211–28. [CrossRef].
6. Li M, Ding Y, Sun J, Lü K, Huang X, Wang J, et al. Research progress and prospect of wellbore cooling technology. Acta Pet Sin. 2025;46(4):789. [CrossRef].
7. Yao L, Quan X, Zhang Y, Huang S, Feng Q, Zhang X. Preparation and performance evaluation of high-temperature polymer nano-plugging agents for water-based drilling fluids systems applicable to unconventional reservoirs. Polymers. 2025;17(5):588. [CrossRef].
8. Kumar A, Savari S, Whitfill DL, Jamison DE. Wellbore strengthening: the less-studied properties of lost-circulation materials. In: Proceedings of the SPE Annual Technical Conference and Exhibition; 2010 Sep 19–22;Florence, Italy. p. SPE-133484-MS. [CrossRef].
9. Cai J, Chenevert ME, Sharma MM, Friedheim J. Decreasing water invasion into atoka shale using nonmodified silica nanoparticles. SPE Drill Complet. 2012;27(1):103–12. [CrossRef].
10. Cheraghian G, Wu Q, Mostofi M, Li MC, Afrand M, Sangwai JS. Effect of a novel clay/silica nanocomposite on water-based drilling fluids: improvements in rheological and filtration properties. Colloids Surf A Physicochem Eng Asp. 2018;555:339–50. [CrossRef].
11. He Z, Xu H, Wang J, Sun J, Liu L, Li W, et al. Molecular dynamics study on the Micro-Mechanism of modified nano-silica for inhibiting shale surface hydration. Fuel. 2025;393:134967. [CrossRef].
12. Hajiabadi SH, Bedrikovetsky P, Mahani H, Khoshsima A, Aghaei H, Kalateh-Aghamohammadi M, et al. Effects of surface modified nanosilica on drilling fluid and formation damage. J Petrol Sci Eng. 2020;194:107559. [CrossRef].
13. Shi J, Yao X, Wang C, Ren T, Liu K, Hao H, et al. Study on synthesis and performance of a hybrid crosslinked composite gel for high-temperature lost circulation control. Gels. 2026;12(4):325. [CrossRef].
14. Lei M, Huang W, Sun J, Shao Z, Chen Z, Chen W. Synthesis and characterization of high-temperature self-crosslinking polymer latexes and their application in water-based drilling fluid. Powder Technol. 2021;389:392–405. [CrossRef].
15. Tabatabaei M, Taleghani AD, Li G, Zhang T. Shape memory polymers as lost circulation materials for sealing wide-opened natural fractures. SPE Drill Complet. 2021;36(4):931–42. [CrossRef].
16. Cui K, Jiang G, Xie C, Yang L, He Y, Shen X, et al. A novel temperature-sensitive expandable lost circulation material based on shape memory epoxy foams to prevent losses in geothermal drilling. Geothermics. 2021;95:102145. [CrossRef].

17. Ma Q, Ren M, Wang C, Xing X, Liu L, Yang W. High performance shape memory epoxy syntactic foam composites as lost circulation material in deep drilling. Macro Mater Eng. 2024;309(3):2300303. [CrossRef].
18. Zhang X, Liu J, Sun J, Wang Z, Dai Z, Sun Y, et al. A novel amphoteric ion-modified, styrene-based nanomicrosphere and its application in drilling fluid. Materials. 2023;16(18):6096. [CrossRef].
19. Singh A, Chauhan A, Gaur R. A comprehensive review on the synthesis, properties, environmental impacts, and chemiluminescence applications of polystyrene (PS). Discover Chem. 2025;2(1):47. [CrossRef].
20. Liu B, Zhang M, Wu G, Zhang H. Synthesis of large-scale, monodisperse latex particles via one-step emulsion polymerization through *in situ* charge neutralization. Colloids Surf A Physicochem Eng Asp. 2016;500:127–36. [CrossRef].
21. Caruso F, Caruso RA, Möhwald H. Production of hollow microspheres from nanostructured composite particles. Chem Mater. 1999;11(11):3309–14. [CrossRef].
22. Gorsd MN, Pizzio LR, Blanco MN. Synthesis and characterization of hollow silica spheres. Procedia Mater Sci. 2015;8:567–76. [CrossRef].
23. Wang H, Peng L, Huang Z, Mei S. Well-dispersed hollow silica microspheres synthesis with silica sol as precursor by template method. J Mol Struct. 2014;1059:15–9. [CrossRef].
24. Mouhamad AW, Elzein T, Barroca-Aubry N, Simoni E, Berri N, Brisset F, et al. Synthesis and characterization of polystyrene-b-poly(vinyldipicolinic acid) pH-responsive core-shell nanoparticles. Eur Polym J. 2023;201:112541. [CrossRef].
25. Lu S, Zhu K, Song W, Song G, Chen D, Hayat T, et al. Impact of water chemistry on surface charge and aggregation of polystyrene microspheres suspensions. Sci Total Environ. 2018;630:951–9. [CrossRef].
26. Zhang C, Sun J, Huang X, Zhang Y, Zong J, Lv K, et al. Use of modified polystyrene micro-nano spheres to improve the inhibition and plugging performance of water-based drilling fluids. Colloids Surf A Physicochem Eng Asp. 2023; 668:131409. [CrossRef].
27. Zeng W, Huang W, Guo B, Sun Y, Shen H. Preparation and lubricating properties of polystyrene composite microspheres. Materials. 2023;16(8):3071. [CrossRef].
28. Khan MA, Lv K, Sun J, Liu F, Shen H, Ding Y, et al. Enhanced filtration performance of cellulose nanofiber/bentonite water-based drilling fluids with temperature- and salt-resistant polymers for extreme conditions. SPE J. 2025;30(9):5327–49. [CrossRef].
29. Yun DS, Lee HS, Jang HG, Yoo JW. Controlling size and distribution for nano-sized polystyrene spheres. Bull Korean Chem Soc. 2010;31(5):1345–8. [CrossRef].
30. Du X, He J. Facile size-controllable syntheses of highly monodisperse polystyrene nano- and microspheres by polyvinylpyrrolidone-mediated emulsifier-free emulsion polymerization. J Appl Polym Sci. 2008;108(3):1755–60. [CrossRef].
31. Kim S, Pyo HB, Ko SH, Ah CS, Kim A, Kim WJ. Fabrication of anionic sulfate-functionalized nanoparticles as an immunosensor by protein immobilization. Langmuir. 2010;26(10):7355–64. [CrossRef].
32. Kishimoto H, Watanabe M, Iyoda T, Nagai K, Nakagawa M. Photocontrol of ζ-potential of poly(styrene) microspheres prepared by soap-free emulsion copolymerization. Chem Lett. 2006;35(6):598–9. [CrossRef].
33. Senses E, Black M, Cunningham T, Sukhishvili SA, Akcora P. Spatial ordering of colloids in a drying aqueous polymer droplet. Langmuir. 2013;29(8):2588–94. [CrossRef].
34. Nie X, Chen J, Cao Y, Zhang J, Zhao W, He Y, et al. Investigation on plugging and profile control of polymer microspheres as a displacement fluid in enhanced oil recovery. Polymers. 2019;11(12):1993. [CrossRef].
35. Lin R, Sun L. Numerical simulation of the microscopic plugging mechanism and particle flow process of the microsphere system. ACS Omega. 2022;7(50):46983–91. [CrossRef].
36. Lin M, Zhang G, Hua Z, Zhao Q, Sun F. Conformation and plugging properties of crosslinked polymer microspheres for profile control. Colloids Surf A Physicochem Eng Asp. 2015;477:49–54. [CrossRef].
37. Dong KJ, Zou RP, Yang RY, Yu AB, Roach G. DEM simulation of cake formation in sedimentation and filtration. Miner Eng. 2009;22(11):921–30. [CrossRef].
38. Yang D, Khan MA, Liao B, Shi X, Lv K, Sun J, et al. Cellulose nanofibers as anti-sagging agents in water-based drilling fluids. Int J Biol Macromol. 2025;322:146779. [CrossRef].
39. Zhang Y, Lv K, Sun J, Liu C, Li MC. Lignin-containing cellulose nanofibers as stabilizers in Pickering emulsion-based drilling fluids. Int J Biol Macromol. 2025;329:147828. [CrossRef].

40. Khan MA, Lv K, Sun J, Shen H, Zhang Y, Noor AA, et al. Influence of salt and temperature on the rheological and filtration properties of cellulose Nanofiber/bentonite water-based drilling fluids. Geoenergy Sci Eng. 2025;244:213524. [CrossRef].

41. Dindoruk B, Ratnakar RR, Suchismita S. Phase behavior modeling of acid-gas aqueous systems CO_2, H_2S, CH_4, water and *in situ* pH measurements in applications to wellbore integrity and top-of-line corrosion. In: Proceedings of the SPE Annual Technical Conference and Exhibition; 2020 Oct 26–29; Virtual. p. D022S061R043. [CrossRef].